Research Article

Yuxin Tan, Yajie Feng, Tingting Yan, Chuanfeng Zang*, and Meixian Li*

Heparin and zwitterion functionalized smalldiameter vascular grafts for thrombogenesis prevention

https://doi.org/10.1515/epoly-2025-0041 received June 27, 2025; accepted September 04, 2025

Abstract: Vascular transplantation is a widely employed surgical approach for treating cardiovascular diseases (CVDs). However, artificial vascular grafts exhibit high thrombogenicity. Consequently, developing grafts with enhanced antithrombotic properties represents a critical strategy for addressing CVD-related complications. In this study, double-layered vascular grafts were fabricated via electrospinning, featuring a polycaprolactone (PCL)/zwitterionic polyurethane (sulfobetaine polyurethane [SBPU]) inner layer and a pure PCL outer layer, followed by covalent heparin modification. Fiber surface morphology and chemical composition were characterized using scanning electron microscopy and Fouriertransform infrared spectroscopy, respectively. Evaluations included contact angle measurement, mechanical testing, protein/platelet adsorption assays, cytotoxicity assessment, and degradation analysis to determine antithrombotic performance and biocompatibility. Results demonstrated that heparin-modified PCL containing 20 wt% SBPU (PCLH/ SBPU20) exhibited exceptional hydrophilicity, potent antithrombotic effects, superior anti-protein adsorption, favorable anticoagulant properties, and non-cytotoxicity. Among all samples, PCLH/SBPU20 demonstrated optimal comprehensive performance, positioning it as a promising candidate for clinical vascular graft applications.

Keywords: polycaprolactone, zwitterionic polyurethane, double-layered small-diameter vascular grafts, electrospinning, thrombogenesis

1 Introduction

The increase in human longevity has been paralleled by a marked rise in the prevalence of cardiovascular pathologies. Among these, atherosclerosis-induced vascular stenosis and thrombosis present significant threats to global health (1,2). Indeed, cardiovascular diseases (CVDs) now represent the most prevalent category of disorders worldwide (3,4). In clinical practice, vascular grafting serves as a primary surgical intervention; however, this procedure is often complicated by thrombus formation within the graft lumen. This complication may lead to vascular occlusion and increased surgical morbidity (5–7). Consequently, developing vascular grafts with improved thromboresistance stands as a pivotal strategy for addressing CVD-related challenges (8).

Vascular grafts require an optimized porous architecture to support critical biological processes such as cell adhesion, proliferation, and nutrient mass transport for functional integration (9,10). Contemporary fabrication methods for porous vascular grafts employ advanced techniques such as electrospinning, bioprinting, lyophilization, particulate leaching, and gas foaming (11). These state-ofthe-art approaches enable the engineering of biopolymeric scaffolds exhibiting diverse structural characteristics. Among them, electrospinning stands out as a particularly promising modality for vascular graft fabrication due to its exceptional capacity to generate fibrous matrices that faithfully recapitulate the natural extracellular matrix (ECM) structure (12,13). Furthermore, electrospinning's established protocols and cost efficiency position it as a leading strategy in vascular tissue engineering.

Current clinically utilized vascular graft materials include expanded polytetrafluoroethylene, polycaprolactone (PCL), polyurethane (PU), polyglycolic acid, poly(lactic acid), and their composite derivatives, each exhibiting advantages and limitations in hemodynamic applications (14–18). Among these, PCL is a promising candidate for artificial vascular grafts due to its high biocompatibility

^{*} Corresponding author: Chuanfeng Zang, School of Textile and Clothing, Nantong University, Nantong, 226019, China, e-mail: zang.cf@ntu.edu.cn

^{*} Corresponding author: Meixian Li, School of Textile and Clothing, Nantong University, Nantong, 226019, China, e-mail: lmx321@ntu.edu.cn Yuxin Tan, Yajie Feng, Tingting Yan: School of Textile and Clothing, Nantong University, Nantong, 226019, China

and electrospinnability, which enables tunable fiber architectures (19,20). Sevost'ianova et al. fabricated electrospun PCL vascular grafts (2 mm inner diameter) with porous fiber structures (fiber diameter: 3.34 ± 0.51 µm), demonstrating superior mechanical strength (1.88 MPa vs 1.26 MPa in bioprostheses) and elasticity (232.1% elongation vs 95.4% in controls), while achieving complete endothelialization and cellular infiltration in rat abdominal aorta models at 6 weeks post-implantation (21). However, PCL has inherent limitations, particularly poor hydrophilicity and limited bioactivity, necessitating complementary functional components to enhance clinical efficacy (8,22,23), PU offers exceptional elasticity and distinct advantages over other synthetic materials (24,25). Microporous PU vascular grafts show superior water permeability, enhanced hemocompatibility, and compliance comparable to native vessels, making them suitable for catheters, implants, and cardiac assist devices (26,27). Mohaddesi et al. engineered PU-reinforced PCL grafts via electrospinning, achieving 232.1% elongation-to-failure and 56.04° hydrophilicity, which reduced platelet adhesion by 45% and enabled full endothelialization within 6 weeks (28).

Despite morphological similarities between electrospun nanofibers and native ECM, their inherent hydrophobicity significantly impedes cellular migration, adhesion, proliferation, and differentiation (29). Consequently, developing vascular grafts with sustained antithrombogenic properties necessitates extensive investigation. In this study, heparin was employed for surface modification of vascular grafts to enhance thromboresistance. Heparin, a linear polysaccharide complex, comprises four saccharide units: glucosamine, L-iduronic acid, N-acetylglucosamine, and D-glucuronic acid (30,31). This biomolecule exhibits the highest negative charge density among biological molecules due to abundant carboxyl and sulfonic acid groups within its structure (32). This charge distribution facilitates chemical and physical modifications while enabling adsorption of molecules that enhance cellular activity (33). Furthermore, heparin critically promotes endothelialization and suppresses excessive smooth muscle cell proliferation, as extensively demonstrated in vitro, in vivo, and during cardiovascular and peripheral vascular surgeries (34,35).

To address persistent challenges in thrombosis and intimal hyperplasia in small-diameter vascular grafts, a double-layered small-diameter vascular grafts were prepared in this study. The inner layer is PCL/zwitterionic polyurethane (sulfobetaine polyurethane [SBPU]) that could reduce protein adsorption and platelet adsorption, while the outer layer is pure PCL that plays a supporting role, and then heparin was covalently grafted onto this

double-layered structure to further enhance hemocompatibility. Through comprehensive characterization and hemocompatibility evaluations including protein adsorption, platelet adhesion, and anticoagulation assays, this integrated design synergistically combines passive antithrombogenic properties with active thromboresistance, offering a clinically viable strategy to overcome limitations of existing grafts.

2 Materials and methods

2.1 Materials

PCL (Mw 45000) and N-(3-dimethylaminopropyl)-N'-ethylcarbodiimide (EDC) were purchased from Macklin (China). Hexafluoroisopropanol (99.5%) and 1,6-hexanediamine were purchased from Aladdin (China). Dulbecco's modified Eagle's medium (DMEM), fetal bovine serum (FBS), and cell counting kit-8 (CCK-8) were purchased from FeiyuBio Co., Ltd. (China). Methanol and ethanol were purchased from Rhawn (China), and chloroform was purchased from SinoPharm (China). The micro-bicinchoninic acid (BCA) assay kit was purchased from CWBio (China), and the lactate dehydrogenase (LDH) activity assay kit was purchased from Solarbio (China). CD-1 mouse whole blood was purchased from SenBeiJia Biological Technology Co., Ltd. (China), and platelet-rich plasma (PRP) preparation solution was purchased from Leagene Biotechnology (China). Lipase was purchased from Bide Pharmatech Ltd.

2.2 Preparation of PCL/SBPU small-diameter artificial vascular grafts

SBPU synthesis commenced with the reaction of N-methyl diethanolamine (0.2 mol) and 1,3-propanesultone (0.2 mol) in dichloromethane under 2 h stirring, followed by 2-day crystallization. The resultant sulfobetaine diol (SBD) was vacuum-filtered, sequentially washed with dichloromethane/isopropanol, and dried for 48 h. Subsequently, SBD (0.01 mol) and methylene diphenyl diisocyanate (0.01 mol) were dissolved in DMSO (30 ml) under N_2 at 80°C. Catalyzed by dropwise addition of dibutyltin dilaurate, polymerization proceeded for 20 min before methanol precipitation and vacuum drying (50°C, 48 h) to yield SBPU. For graft fabrication, double-layered vascular grafts (5 mm) with varying SBPU content (0, 5, 10, 20 wt%)

were electrospun: the inner layer (PCL/SBPU blend) at 18 kV, 20 cm collector distance, and 1 mL·h⁻¹ flow rate, while the outer layer (pure PCL) at 12 kV, 20 cm, and 1.5 mL·h⁻¹. These were designated as PCL, PCL/SBPU5, PCL/SBPU10, and PCL/SBPU20, respectively.

2.3 Heparin modification of PCL/SBPU small aperture artificial vascular grafts

All samples (PCL, PCL/SBPU5, PCL/SBPU10, PCL/SBPU20) first underwent amination by immersion in 0.43 g·mL⁻¹ 1,6-hexanediamine/isopropanol at 37°C. Subsequently, heparin (1 mg·mL⁻¹) was activated in 2-(N-morpholino)ethanesulfonic acid buffer (0.05 M, pH 5.0) containing 0.3 mol·L⁻¹ EDC and 0.15 mol·L⁻¹ N-hydroxysuccinimide (37°C, 30 min), followed by grafting the aminated samples in this solution for 24 h at 37°C. Finally, samples were rinsed thrice with deionized water and freeze-dried for 24 h (36.37), vielding heparin-modified small-diameter vascular grafts designated PCLH, PCLH/SBPU5, PCLH/SBPU10, and PCLH/SBPU20.

2.4 Characterization

The synthesized SBD was subjected to nuclear magnetic resonance (NMR) spectroscopy (Bruke, Switzerland). The samples with 1 w/v% concentration were prepared using deuterated dimethyl sulfoxide (DMSO- d_6), and ¹H NMR spectra ranged from 0 to 10 ppm. The surface morphology of grafts was observed by field-emission scanning electron microscopy (JSM-6510, JEOL Ltd., Japan) with an accelerating voltage of 5 kV. The chemical structure of the grafts was analyzed using Fourier-transform infrared spectroscopy (FI-TR, Nicoiet IS, Yixiang Instrument Co., Ltd., China).

2.5 Water contact angle assay

The hydrophilicity of vascular grafts was evaluated using an optical contact angle instrument (OCA1SEC, DPT GMBH). Surface hydrophilicity of PCLH, PCLH/SBPU5, PCLH/ SBPU10, and PCLH/SBPU20 was determined via static and dynamic contact angle methods. Samples were sectioned to expose the inner wall for measurement. Three distilled water droplets were placed at different surface locations to measure contact angles.

2.6 Analysis of mechanical properties

The tensile properties of PCLH, PCLH/SBPU5, PCLH/SBPU10, and PCLH/SBPU20 were evaluated using an Instron 5969 universal testing system. Specimens measured 5 mm in diameter and 5 cm in length, with a gauge length of 3 cm and a crosshead speed of 50 mm·min⁻¹. Each sample was stretched until fracture, recording both the stress-strain curve and fracture strength.

2.7 Degradation assay

Four specimens each of PCLH, PCLH/SBPU5, PCLH/SBPU10, and PCLH/SBPU20 were dried to constant weight. Each sample was sectioned to 1 cm length, weighed, numbered sequentially, and the pre-degradation weight recorded as W_0 . Specimens were immersed in phosphate-buffered saline (PBS) containing 200 U·mL⁻¹ lipase, retrieved at intervals, rinsed thrice with deionized water, dried to constant weight, and reweighed to obtain degraded mass (W_1) . Weight loss rates were calculated using Eq. 1 (38):

Weight loss(%) =
$$\frac{W_0 - W_1}{W_0} \times 100\%$$
 (1)

2.8 Platelet adsorption assay

Samples were sectioned into 1 cm × 1 cm pieces, placed in 24-well plates, disinfected with 70% ethanol and UV light for 10 min, and hydrated in PBS at 37°C for 1 h. The solution was then removed; 1 mL of platelet solution was added to each well and incubated at 37°C for 2 h. After removing the platelet solution and washing with PBS three times, 2% Triton X-100 solution was added, followed by incubation at 37°C for 15 min. Absorbance was finally measured at 450 nm using a microplate reader (39,40).

2.9 Protein adsorption assay

Samples were sectioned into 1 cm × 1 cm pieces and placed in 24-well plates. After adding 1 mL of PBS to each well and equilibrating at room temperature for 2h, PBS was aspirated. Then, 1 mL of either 2 mg·mL⁻¹ bovine serum albumin (BSA) or $0.1\,\mathrm{mg}\cdot\mathrm{mL}^{-1}$ fibrinogen (Fg) solution was added per well and incubated with shaking at 37°C for 1h. Following protein solution aspiration and PBS

addition, samples were rinsed via repeated pipetting (three cycles). Subsequently, 1 mL of 2 wt% SDS solution was added to each well and incubated with shaking at 37°C for 2 h. Then, 0.1 mL aliquots of SDS solution were transferred from each well to a 96-well plate. After adding BCA solution to each well, the foil-wrapped plate was incubated at 37°C for 1–2 h. Absorbance was finally measured at 562 nm using a microplate reader (41,42).

2.10 Coagulation assay

Samples were sectioned into circular sheets measuring 14 mm in diameter. For each experimental group, three replicate specimens were prepared and positioned in 24well plates, with glass slides designated as positive controls. Each well received 100 µL of whole blood supplemented with 20 μ L CaCl, (0.2 mol·L⁻¹), followed by incubation at 37°C. After 1 h, the test materials were removed; 2.5 mL deionized water was introduced and incubated at 37°C for 5 min. The resulting supernatant was transferred to centrifuge tubes, homogenized by vortex mixing at room temperature for 15 min, and the absorbance was measured at 540 nm. Elevated absorbance values directly indicate increased hemoglobin concentration in the supernatant, demonstrating greater quantities of free blood cells and correspondingly reduced clotted cell populations. This inverse relationship signifies slower coagulation kinetics. Consequently, higher supernatant absorbance correlates with elevated coagulation indices, reflecting superior anticoagulant properties of the biomaterial (43). Blood clotting index (BCI) is calculated according to the following Eq. 2:

$$BCI(\%) = \frac{I_t}{I_w} \times 100\%$$
 (2)

where the absorbance value of the sample under test is denoted as $I_{\rm b}$ and $I_{\rm w}$ is the absorbance value of the mixed solution obtained by 2.5 mL deionized water and 100 μ L whole blood (44).

2.11 Cytotoxicity assay

Samples were sectioned to dimensions of 1 cm \times 3 cm, sterilized via UV irradiation for 24 h, and subsequently immersed in PBS for \geq 24 h to eliminate residual contaminants. L929 fibroblast cells were maintained in DMEM supplemented with 10% FBS at 37°C under 5% CO₂. Sterilized graft samples (ethanol-immersed and UV-irradiated) were incubated in serum-free DMEM at an extraction ratio of

3 cm²·mL⁻¹ for 24 h at 37°C. The resulting extracts were then applied to cell monolayers for 24 h exposure. Cell viability was quantified via CCK-8 assay, measuring absorbance at 450 nm with 10% DMSO and plain DMEM serving as positive/negative controls, respectively (45,46). The cell viability was calculated according to the following Eq. 3:

Cell viability(%) =
$$\frac{OD_{sample} - OD_{blank}}{OD_{control} - OD_{blank}} \times 100\%$$
 (3)

2.12 Statistical analysis

All the experiments were done independently in three replicates, and the data were stated as mean value \pm standard deviation. The one-way analysis of variance (ANOVA) and Tukey's multiple comparison tests were used to analyze the significance of differences between experimental groups. A value of $p^* < 0.05$ and $p^{**} < 0.01$ was considered to be statistically significant. In this study, the analysis of tensile strength and cell viability data was conducted using ANOVA.

3 Results and discussions

3.1 Nuclear magnetic resonance test (¹H NMR)

To confirm the successful synthesis of SBD, the chemical structure of the artificial vascular material was systematically characterized by NMR analysis using DMSO- d_6 as the solvent (Figure 1). Resonances at 3.82 ppm were assigned to the urethane linkage, while those spanning 2.1–4.6 ppm corresponded to the methyl and methylene protons of the SB moiety. Collectively, these findings confirm the successful synthesis of SBPU.

3.2 Analysis of infrared spectral analysis

FT-IR spectra of the scaffolds are presented in Figure 2. All samples exhibited characteristic absorption peaks at approximately 1,720 and 1,171 cm⁻¹, corresponding to C=O and C-O-C stretching vibrations, respectively (28,47). A distinctive peak at ~2,950 cm⁻¹, characteristic of PCL, was observed in all cases, confirming retention of PCL's chemical integrity following incorporation of SBPU and heparin. In this study, heparin was covalently immobilized onto the PCL/SBPU matrix to provide sustained anticoagulant functionality while avoiding burst release issues

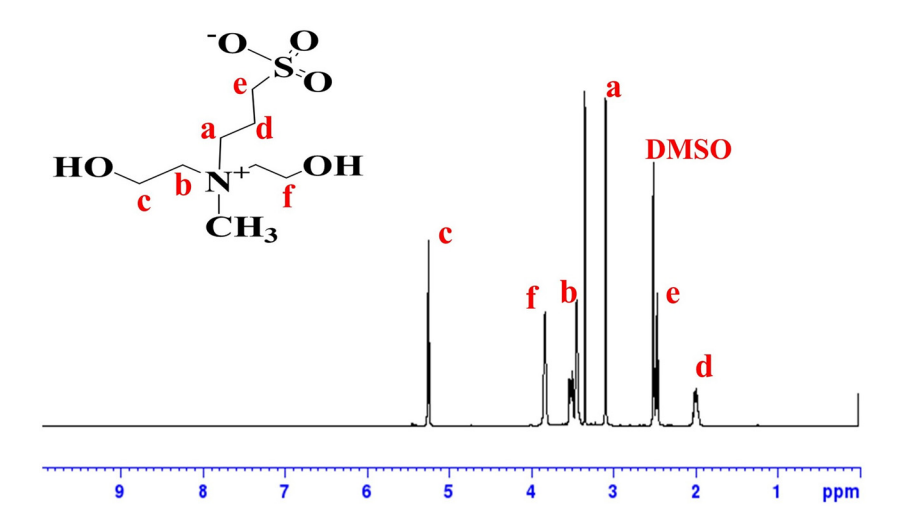


Figure 1: ¹H NMR spectra of SBD.

inherent to physical blending methods. Characteristic heparin absorption peaks appeared at 3,300-3,500 cm⁻¹ (N-H and O-H stretching vibrations) (37,44). All four spectra displayed defined peaks at 3,265 cm⁻¹, verifying successful heparin grafting onto sample surfaces. Additionally, SBD spectra showed broad bands within 3,200-3,500 cm⁻¹ (O-H stretching) (39).

presented in Figure 3. Panels (a) through (d), respectively, display SEM images of these four material variants. Notably, SBPU incorporation induces significant alterations in fiber surface smoothness, with the magnitude of this effect being concentration-dependent. Corresponding fiber diameter distributions are shown in panels (e)-(h), revealing that increasing SBPU content progressively broadens the diameter distribution profile.

3.3 Analysis of scanning electron microscope (SEM)

The micromorphology and diameter distributions of PCLH, PCLH/SBPU5, PCLH/SBPU10, and PCLH/SBPU20 samples are

3.4 Analysis of water contact angle assay

The hydrophilic properties and wettability of vascular grafts constitute critical determinants influencing cellular

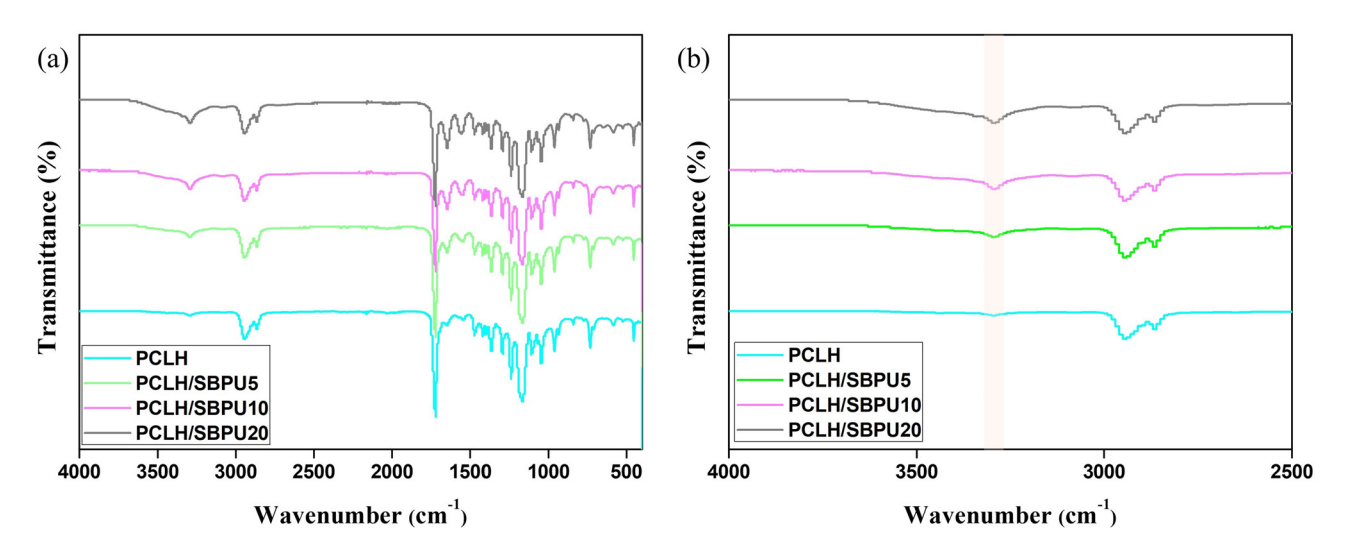


Figure 2: (a) FT-IR spectra of PCLH, PCLH/SBPU5, PCLH/SBPU10, PCLH/SBPU20, (b) enlarged FT-IR spectra of PCLH, PCLH/SBPU5, PCLH/SBPU10, PCLH/SBPU5, PC SBPU20.

6 — Yuxin Tan et al. DE GRUYTER

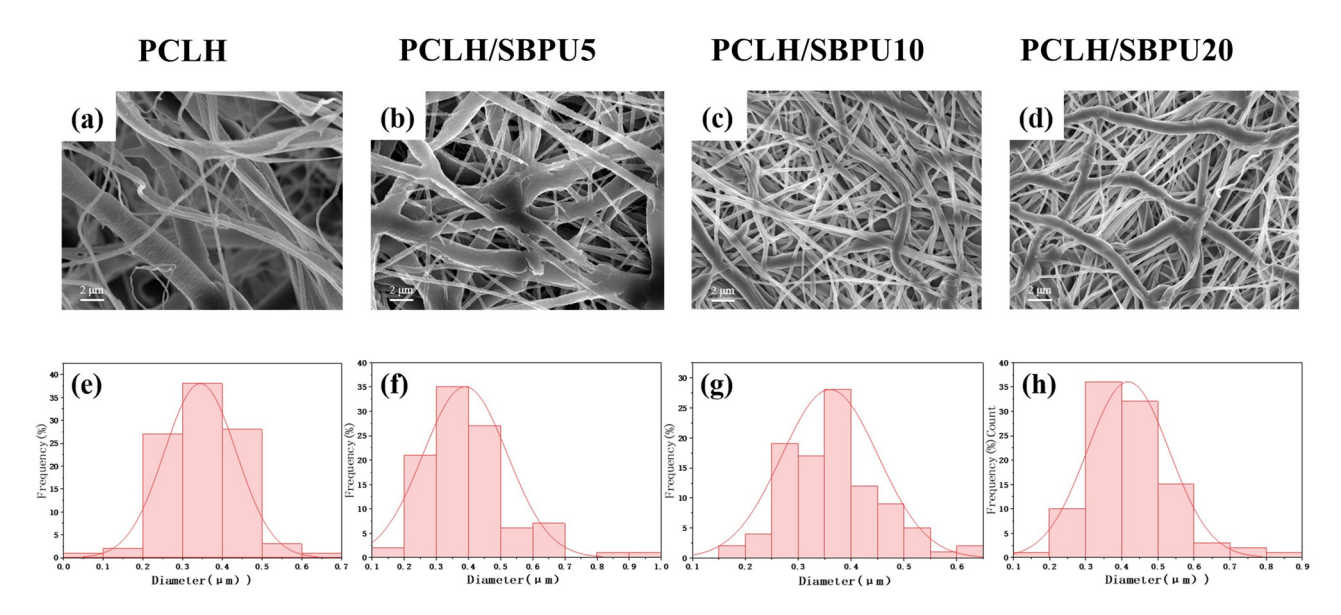


Figure 3: (a)–(d) Scanning electron micrographs of PCLH, PCLH/SBPU5, PCLH/SBPU10, PCLH/SBPU20, respectively. (e)–(h) Corresponding diameter distributions of PCLH, PCLH/SBPU5, PCLH/SBPU10, PCLH/SBPU20.

adhesion, infiltration, and proliferation (48). Dynamic contact angle analysis quantifies material hydrophilicity through temporal measurements from initial liquid contact to complete wetting. As shown in Figure 4, heparin-modified grafts demonstrated significantly enhanced hydrophilicity, achieving complete liquid wetting within 0.43 s (49). The blending of PCL with SBPU revealed composition-dependent wettability characteristics. Incorporation of SBPU prolonged

wetting duration, most notably in the 10 wt% PCLH-SBPU composite which exhibited the longest wetting time (4.79 s). This effect may be attributed to surface roughness modifications induced by SBPU addition that temporarily reduced hydrophilicity. In contrast, at 20 wt% SBPU loading, complete wetting time decreased significantly to 1.2 s. This reversal phenomenon stems from increased density of hydrophilic functional groups (ester linkages C=O and aldehyde groups

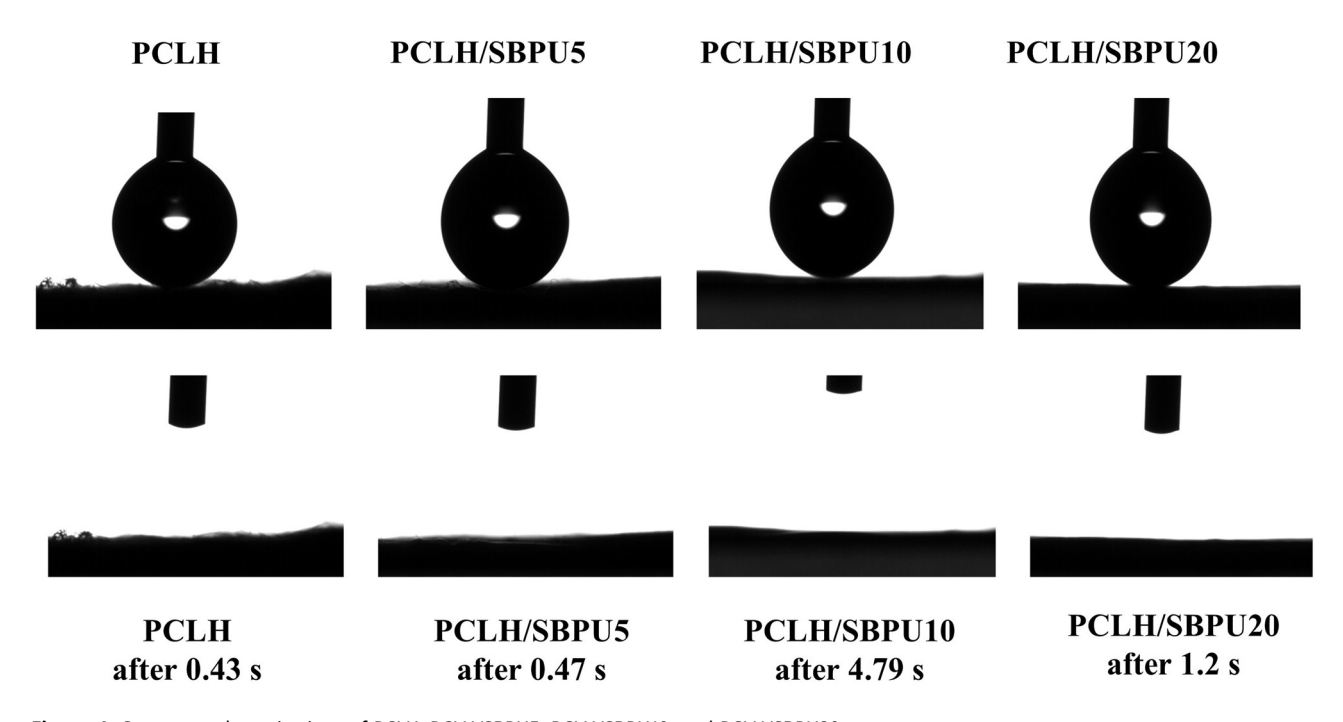


Figure 4: Contact angle projections of PCLH, PCLH/SBPU5, PCLH/SBPU10, and PCLH/SBPU20.

–CHO) within the graft matrix at higher SBPU concentrations, enhancing surface hydrophilicity through strengthened polar interactions with aqueous media.

3.5 Analysis of mechanical properties

Uniaxial tensile testing evaluated the mechanical properties of vascular grafts to ensure adequate post-implantation mechanical stability (50,51). Figure 5 demonstrates that fracture strengths of SBPU-incorporated samples (3.17, 3.79, 4.49 MPa) significantly exceeded the PCLH control (1.72 MPa). This indicates that SBPU enhances tensile strength proportionally to its concentration. The mechanical improvement likely stems from structural differences between SBPU and PCLH molecules, where SBPU's integration into PCLH chains modifies material behavior. Furthermore, increasing SBPU content correspondingly elevated strain tolerance, demonstrating concentration-dependent ductility enhancement.

3.6 Analysis of degradation assay

Enzymatic degradation was evaluated in lipase-containing PBS (200 U·mL⁻¹). Figure 6 displays time-dependent weight loss profiles for PCLH, PCLH/SBPU5, PCLH/SBPU10, and PCLH/SBPU20. PCLH underwent rapid degradation with >95% mass loss within 3 days, indicating accelerated enzymatic hydrolysis that potentially compromises cellular

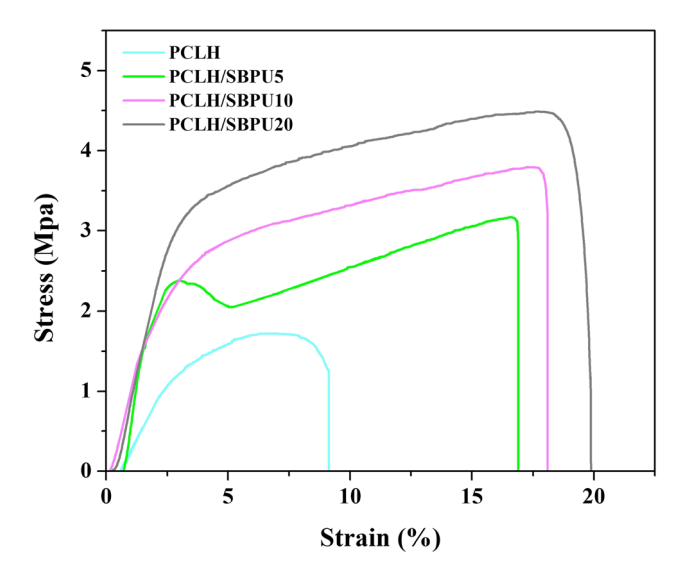


Figure 5: Tensile stress–strain curves of PCLH, PCLH/SBPU5, PCLH/SBPU10, and PCLH/SBPU20.

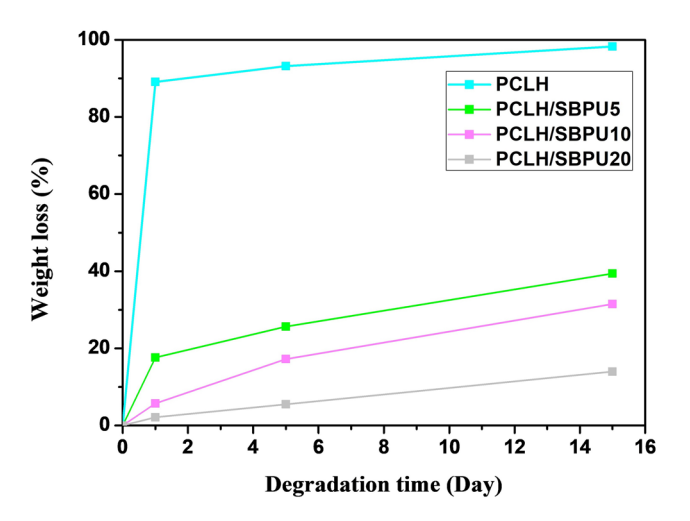


Figure 6: Weight loss rate of four groups of samples PCLH, PCLH/SBPU5, PCLH/SBPU10, and PCLH/SBPU20.

integration in vascular grafts. Conversely, SBPU-incorporated composites exhibited significantly retarded degradation kinetics. After initial degradation, PCLH/SBPU5, PCLH/SBPU10, and PCLH/SBPU20 reached weight loss equilibrium, demonstrating an inverse correlation between residual mass and SBPU content. Notably, PCLH/SBPU20 achieved only 15% total mass loss, confirming composition-dependent degradation resistance.

This stabilization confirms SBPU effectively modulates PCLH degradation kinetics, enabling prolonged structural—mechanical stability essential for vascular graft performance. The underlying mechanism likely involves SBPU's superior hydrolysis resistance compared to PCL, attributable to strengthened interchain bonding within the composite matrix. These modifications promote endothelial cell adhesion and angiogenesis by maintaining scaffold integrity, consequently supporting long-term patency.

3.7 Analysis of platelet adsorption assay

As shown in Figure 7, L-LDH activity values for SBPU-modified samples were consistently lower than the PCLH control group, indicating progressive enhancement of antiplatelet performance with increasing SBPU content. At 5 wt % SBPU loading, L-LDH activity remained comparable to PCLH. However, significant reductions occurred at 10 and 20 wt% concentrations, with PCLH/SBPU20 exhibiting the lowest activity (5.88 U·mL⁻¹). These results demonstrate superior antiplatelet properties in PCLH/SBPU10 and PCLH/SBPU20 composites. The underlying mechanism likely involves SBPU-mediated suppression of platelet adhesion and activation on the vascular graft surfaces.

3.8 Analysis of protein adsorption assay

Protein adsorption experiments assessed vascular graft protein affinity to predict biocompatibility and potential immune responses in clinical applications (52). Figure 8 shows BSA and Fg adsorption profiles across the four sample groups. Results demonstrate reduced protein adsorption with SBPU incorporation compared to PCLH controls, showing progressive attenuation proportional to SBPU content. This concentration-dependent reduction confirms SBPU enhances the material's anti-protein adsorption efficacy.

3.9 Analysis of coagulation assay

The coagulation index (BCI) at designated timepoints reflects material anticoagulant capacity. Figure 9 presents 1-h BCI results for four vascular graft groups. PCLH samples exhibited comparatively low BCI values after 1-h coagulation. With increasing SBPU content (5–20 wt%), the coagulation index demonstrated progressive elevation proportional to SBPU concentration. While PCLH/SBPU5 showed minimal BCI deviation from PCLH controls, PCLH/SBPU10 and PCLH/SBPU20 composites displayed

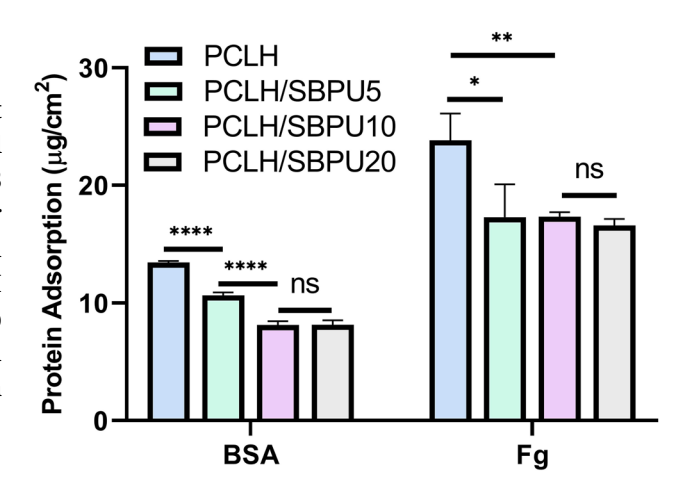


Figure 8: PCLH, PCLH/SBPU5, PCLH/SBPU10, and PCLH/SBPU20 four groups of samples (a) BSA protein adsorption and (b) Fg protein adsorption.

significantly enhanced indices. This concentration-dependent enhancement confirms superior anticoagulant performance at higher SBPU loadings.

3.10 Analysis of cytotoxicity assay

Figure 10 results confirm cell viability exceeding 80% for all PCLH, PCLH/SBPU5, PCLH/SBPU10, and PCLH/SBPU20

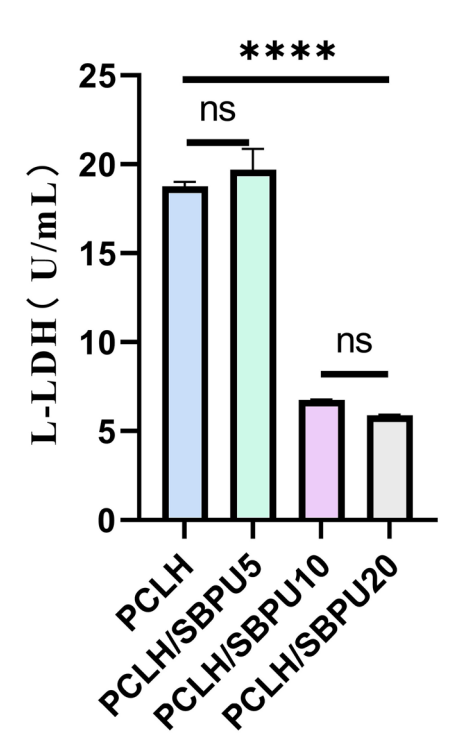


Figure 7: L-LDH viability values for four groups of samples PCLH, PCLH/SBPU5, PCLH/SBPU10, and PCLH/SBPU20.

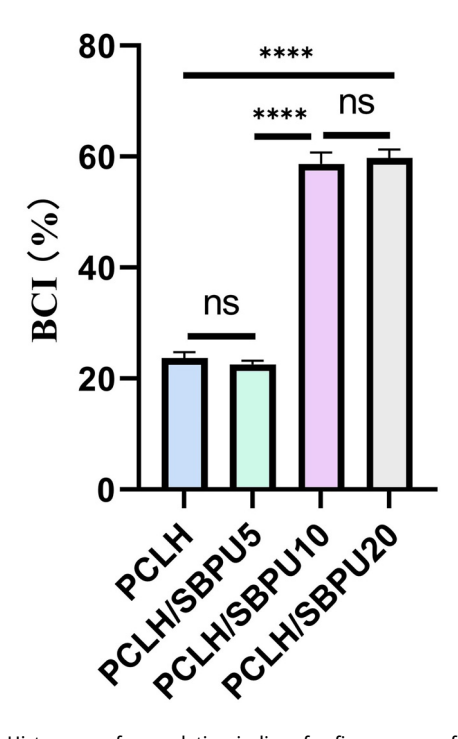


Figure 9: Histogram of coagulation indices for five groups of samples, positive control, PCLH, PCLH/SBPU5, PCLH/SBPU10, and PCLH/SBPU20.

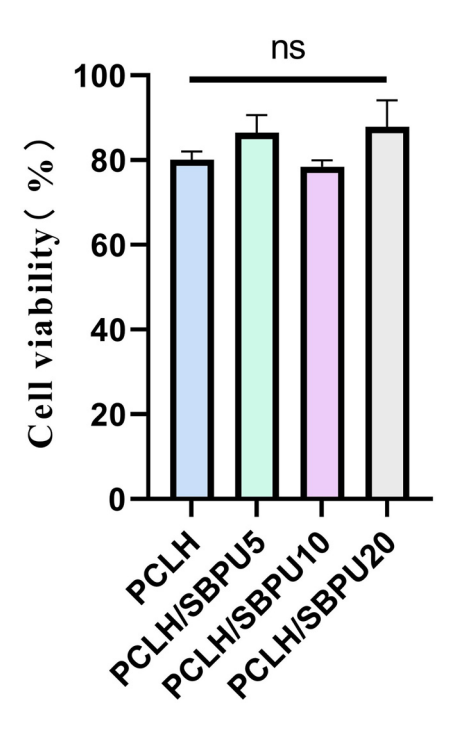


Figure 10: Cell viability of four groups of samples PCLH, PCLH/SBPU5, PCLH/SBPU10, and PCLH/SBPU20.

samples. This demonstrates that SBPU incorporation and heparin modification induce no cytotoxic effects in PCL small-diameter vascular grafts. All four graft variants exhibit inherent biocompatibility, consequently supporting unimpeded cellular proliferation.

4 Conclusion

This study fabricated a double-layered vascular graft via electrospinning, featuring a PCL/SBPU inner layer and a PCL outer layer, with subsequent covalent heparin modification. Comprehensive analysis characterized chemical structure, microstructure, mechanical properties, and antithrombotic performance. Results demonstrated that SBPU incorporation preserved PCL's functional groups, maintaining PCL's fundamental chemical composition. However, SBPU introduction moderately influenced fiber surface topography and diameter distribution. Specifically, SBPU addition induced fiber surface roughening and broadened diameter dispersity. Heparin-modified grafts exhibited pronounced hydrophilicity, which persisted despite SBPU incorporation. Furthermore, SBPU enhanced fracture strength proportionally to its concentration. Critically, SBPU attenuated PCLH degradation rates, enabling prolonged morphological and mechanical stability - essential for vascular graft functionality. Compared to PCLH controls, SBPU-incorporated composites demonstrated superior antiprotein adsorption, reduced platelet adhesion, and enhanced biocompatibility. Coagulation assays revealed progressive elevation of coagulation indices with increasing SBPU concentrations, confirming concentration-dependent anticoagulant enhancement.

Collectively, PCLH/SBPU20 exhibited optimal multifunctionality: high hydrophilicity, robust tensile strength, exceptional antithrombotic efficacy, unparalleled anti-protein adsorption, potent anticoagulation, and non-toxicity. This composite demonstrated superior overall performance relative to other formulations, establishing significant translational potential for small-diameter vascular grafts.

Funding information: This work was supported by the Key R&D project of Jiangsu Province (BE2023740), Natural Science Foundation of Jiangsu Province (BK20220613), College Students' Innovation and Entrepreneurship Training Program (X202510304314).

Author contributions: Conceptualization, methodology, and validation: Yuxin Tan, Yajie Feng; formal analysis: Yuxin Tan, Tingting Yan.; writing – original draft preparation: Yuxin Tan; writing - review and editing: Yuxin Tan, Meixian Li.; supervision, project administration: Chuanfeng Zang, Meixian Li. All authors have read and agreed to the published version of the manuscript.

Conflict of interest: Authors state no conflict of interest.

References

- Rashid B. Glasser MF. Nichols T. Van Essen D. luttukonda MR. Schwab NA, et al. Cardiovascular and metabolic health is associated with functional brain connectivity in middle-aged and older adults: Results from the Human Connectome Project-Aging study. Neuroimage. 2023;276:120192.
- Pashneh-Tala S, MacNeil S, Claeyssens F. The tissue-engineered (2) vascular graft—past, present, and future. Tissue Eng Part B Rev. 2015;22:68-100.
- Report on Cardiovascular Health and Diseases in China 2023: An (3) Updated Summary. BES 2024;37:949-92.
- Dalakoti M, Lin NHY, Yap J, Cader A, Dipanker P, Lee D, et al. (4) Primary prevention of cardiovascular disease in asia: opportunities and solutions: a narrative review. JACC: Adv. 2025;4:101676.
- Ding X, Sha D, Sun K, Fan Y. Biomechanical insights into the (5) development and optimization of small-diameter vascular grafts. Acta Biomater. 2025;25:00270-3.
- (6) Abdul Halim R, Challita C, Omeirat N, Kanafani ZA. Vascular graft infections: updates on a challenging problem. Infect Dis Clin N Am. 2024;38:657-71.
- Lang Z, Chen T, Zhu S, Wu X, Wu Y, Miao X, et al. Construction of vascular grafts based on tissue-engineered scaffolds. MTB. 2024;29:101336.

- (8) Teng Y, Xu Y, Lv P, Song L, Yang J, Wang X, et al. Therapeutic strategies for small-diameter vascular graft calcification. Chem Eng J. 2024;487:150549.
- (9) Wang N, Wang H, Weng D, Wang Y, Yu L, Wang F, et al. Nanomaterials for small diameter vascular grafts: overview and outlook. Nanoscale Adv. 2023;5:6751–67.
- (10) Hu K, Li Y, Ke Z, Yang H, Lu C, Li Y, et al. History, progress and future challenges of artificial blood vessels: a narrative review. Biomater Transl. 2022;3:81–98.
- (11) Meng C, Song J, Malekmohammadi S, Meng J, Wei W, Li R, et al. Hierarchical porous poly (L-lactic acid) fibrous vascular graft with controllable architectures and stable structure. Mater Des. 2024:240:112829.
- (12) He Q, Huang C, Lu Y, Zhao Y, Xing M, Wang X, et al. Developing an anticoagulant microfibrous vascular graft with enhanced kink resistance and self-sealing capabilities. Mat Sci Eng C-Mater. 2025:173:214290.
- (13) Xiang P, Li M, Zhang CY, Chen DL, Zhou ZH. Cytocompatibility of electrospun nanofiber tubular scaffolds for small diameter tissue engineering blood vessels. Int | Biol Macromol. 2011;49:281–8.
- (14) Kirkton RD, Prichard HL, Santiago-Maysonet M, Niklason LE, Lawson JH, Dahl SLM. Susceptibility of ePTFE vascular grafts and bioengineered human acellular vessels to infection. J Surg Res. 2018;221:143–51.
- (15) Sun Q, Si J, Zhao L, Wei T, Wang T, Li F, et al. Direct thrombin inhibitor-bivalirudin improved the hemocompatibility of electrospun polycaprolactone vascular grafts. Compos Part B-Eng. 2022;234:109702.
- (16) Li S, Yang L, Zhao Z, Yang X, Lv H. A polyurethane-based hydrophilic elastomer with multi-biological functions for small-diameter vascular grafts. Acta Biomater. 2024;176:234–49.
- (17) Huang AH, Niklason LE. Engineering biological-based vascular grafts using a pulsatile bioreactor. Jove-J Vis Exp. 2011;14:2646–52.
- (18) Liu H, Li X, Niu X, Zhou G, Li P, Fan Y. Improved hemocompatibility and endothelialization of vascular grafts by covalent immobilization of sulfated silk fibroin on poly(lactic-co-glycolic acid) scaffolds. Biomacro. 2011;12:2914–24.
- (19) Kang H, Yan G, Zhang W, Xu J, Guo J, Yang J, et al. Impaired endothelial cell proliferative, migratory, and adhesive abilities are associated with the slow endothelialization of polycaprolactone vascular grafts implanted into a hypercholesterolemia rat model. Acta Biomater. 2022;149:233–47.
- (20) Ntrivala MA, Pitsavas AC, Lazaridou K, Baziakou Z, Karavasili D, Papadimitriou M, et al. Polycaprolactone (PCL): the biodegradable polyester shaping the future of materials – a review on synthesis, properties, biodegradation, applications and future perspectives. Eur Polym J. 2025;234:114033.
- (21) Sevost'ianova VV, Elgudin Ia A, Glushkova TV, Wnek G, Liubysheva T, Emancipator S, et al. Use of polycaprolactone grafts for small-diameter blood vessels. Angiologiia i sosudistaia khirurqiia = Angiology Vasc Surg. 2015;21:44–53.
- (22) Lu X, Zou H, Liao X, Xiong Y, Hu X, Cao J, et al. Construction of PCL-collagen@PCL@PCL-gelatin three-layer small diameter artificial vascular grafts by electrospinning. Biomed Mater. 2022;18:015008.
- (23) Bai S, Zhang X, Zang L, Yang S, Chen X, Yuan X. Electrospinning of biomaterials for vascular regeneration. Chem Res Chin Univ. 2021;37:394–403.
- (24) Zhang B, Xu Y, Ma S, Wang L, Liu C, Xu W, et al. Small-diameter polyurethane vascular graft with high strength and excellent compliance. J Mech Behav Biomed Mater. 2021;121:104614.

- (25) Wu S, Ma S, Zhang Q, Yang C. A comprehensive review of polyurethane: Properties, applications and future perspectives. Polymer. 2025;327:128361.
- (26) Huang H-G, Xiang T, Chen Y-X. Current strategies of surface modifications to polyurethane biomaterials for vascular grafts. Chin Med Sci J. 2023;38:279–85.
- (27) Zhen L, Creason SA, Simonovsky FI, Snyder JM, Lindhartsen SL, Mecwan MM, et al. Precision-porous polyurethane elastomers engineered for application in pro-healing vascular grafts: Synthesis, fabrication and detailed biocompatibility assessment. Biomaterials. 2021;279:121174.
- (28) Mohaddesi M, Jahani A, Vahedi E, Nakhaei M, Ebrahimzadeh MH, Moradi A, et al. Creating and evaluating a novel small diameter PCL/PU vascular graft for finger reconstruction: A comprehensive analysis of structural, mechanical, in vitro, and in vivo assessments. Mater Today Commun. 2024;40:109427.
- (29) Wang Y, Yue G, Bai T, Liu F, Wang N, Bai J, et al. Hierarchical assembly of electrospun nanofibers for the next generation tissue repairing materials. Sustainable MaterTechnol. 2025;44:e01355.
- (30) Li X, Tang J, Bao L, Chen L, Hong FF. Performance improvements of the BNC tubes from unique double-silicone-tube bioreactors by introducing chitosan and heparin for application as small-diameter artificial blood vessels. Carbohydr Polym. 2017;178:394–405.
- (31) Wu M, Sapin-Minet A, Gaucher C. Heparin, an active excipient to carry biosignal molecules: Applications in tissue engineering - A review. Int J Biol Macromol. 2025;312:143959.
- (32) Qiu H, Qi P, Liu J, Yang Y, Tan X, Xiao Y, et al. Biomimetic engineering endothelium-like coating on cardiovascular stent through heparin and nitric oxide-generating compound synergistic modification strategy. Biomaterials. 2019;207:10–22.
- (33) Li C, Wang F, Ge P, Mao Y, Wang L. Anti-acute thrombogenic surface using coaxial electrospraying coating for vascular graft application. Mater Lett. 2017;205:15–9.
- (34) Jiang Y, Wang H, Wang X, Li Q. Surface modification with hydrophilic and heparin-loaded coating for endothelialization and anticoagulation promotion of vascular scaffold. Int J Biol Macromol. 2022;219:1146–54.
- (35) Shokri N, Elahimanesh M, Bakhshandeh M, Najafi M. Heparin suppresses FoxO1/pFoxO1 signaling axis in vascular smooth muscle cells. Biochem Biophys Rep. 2025;41:101954.
- (36) Sun M, Deng J, Gao C. The correlation between fibronectin adsorption and attachment of vascular cells on heparinized polycaprolactone membrane. J Colloid Interface Sci. 2015;448:231–7.
- (37) Li C, Mao J, Li Q, Wang F, Jiao Y, Zhang Z, et al. Long-term anticoagulation and selective cells adhesion surface via combination of covalent grafting and layer by layer assembly. Biomed Mater. 2019;14:065012.
- (38) Han X, Gao Y, Ding Y. In vitro performance of 3D printed PCL-β-TCP degradable spinal fusion cage. J Biomater Appl. 2021;35:1304–14.
- (39) Choi S-Y, Li M-X, Kang JH, Yang DH, Joung YK. Anti-thrombotic polymer surfaces modified with zwitterionic and fluorinated surface-migrating oligomers. Surf Interfaces. 2021;25:101280.
- (40) Dong X, Yuan X, Wang L, Liu J, Midgley AC, Wang Z, et al. Construction of a bilayered vascular graft with smooth internal surface for improved hemocompatibility and endothelial cell monolayer formation. Biomaterials. 2018;181:1–14.
- (41) Cao J, Yang M, Lu A, Zhai S, Chen Y, Luo X. Polyurethanes containing zwitterionic sulfobetaines and their molecular chain rearrangement in water. J Biomed Mater Res Part A. 2013;101:909–18.

- (42) Gao Y, Bai S, Zhu K. Electrospun membranes of diselenidecontaining poly(ester urethane)urea for in situ catalytic generation of nitric oxide. J Biomater Sci Polym Ed. 2024;35:1157–76.
- (43) Yao Y, Wang J, Cui Y, Xu R, Wang Z, Zhang J, et al. Effect of sustained heparin release from PCL/chitosan hybrid small-diameter vascular grafts on anti-thrombogenic property and endothelialization. Acta Biomater. 2014;10:2739–49.
- (44) Li Q, Mu L, Zhang F, Mo Z, Jin C, Qi W. Manufacture and property research of heparin grafted electrospinning PCU artificial vascular scaffolds. Mater Sci Eng C Mater Biol Appl. 2017;78:854–61.
- (45) Mercado-Pagán ÁE, Stahl AM, Ramseier ML, Behn AW, Yang Y. Synthesis and characterization of polycaprolactone urethane hollow fiber membranes as small diameter vascular grafts. Mater Sci Eng C Mater Biol Appl. 2016;64:61–73.
- (46) Seon GM, Lee MH, Kwon BJ, Kim MS, Koo MA, Seomun Y, et al. Recombinant batroxobin-coated nonwoven chitosan as hemostatic dressing for initial hemorrhage control. Int J Biol Macromol. 2018;113:757–63.
- (47) Stefanović IS, Džunuzović JV, Džunuzović ES, Stevanović S, Dapčević A, Savić SI, et al. The impact of the polycaprolactone content on the properties of polyurethane networks. Mater Today Commun. 2023;35:105721.

- (48) Lee J-H, Kwon J-S, Kim Y-H, Choi E-H, Kim K-M, Kim K-N. The effects of enhancing the surface energy of a polystyrene plate by air atmospheric pressure plasma jet on early attachment of fibroblast under moving incubation. Thin Solid Films. 2013;547:99–105.
- (49) Shi J, Chen S, Wang L, Zhang X, Gao J, Jiang L, et al. Rapid endothelialization and controlled smooth muscle regeneration by electrospun heparin-loaded polycaprolactone/gelatin hybrid vascular grafts. J Biomed Mater Res B. 2019;107:2040–9.
- (50) Chen W, Xiao W, Liu X, Yuan P, Zhang S, Wang Y, et al. Pharmacological manipulation of macrophage autophagy effectively rejuvenates the regenerative potential of biodegrading vascular graft in aging body. Bioact Mater. 2022:11:283–99.
- (51) Yang S, Zheng X, Qian M, Wang H, Wang F, Wei Y, et al. Nitratefunctionalized poly(ε-Caprolactone) small-diameter vascular grafts enhance vascular regeneration via sustained release of nitric oxide. Front Bioeng Biotechnol. 2021;9:770121.
- (52) Saleh AH, Borhan G, Goujon F, Devémy J, Dequidt A, Malfreyt P, et al. Molecular and Energetic Descriptions of the Plasma Protein Adsorption onto the PVC Surface: Implications for Biocompatibility in Medical Devices. ACS Omega. 2024;9:38054–65.